ChemPubSoc Europe

DOI: 10.1002/cbic.201500485

CHEMBIOCHEM Full Papers

A Covalent Cysteine-Targeting Kinase Inhibitor of Ire1 Permits Allosteric Control of Endoribonuclease Activity

Daniel D. Waller,*[a, b] Gregor Jansen,[b] Makan Golizeh,[c] Chloe Martel-Lorion,[b] Kurt Dejgaard,[b] Tze Chieh Shiao,[c] John Mancuso,[d] Youla S. Tsantrizos,[d] René Roy,[c] Michael Sebag,[a] Lekha Sleno,[c] and David Y. Thomas[b]

The unfolded protein response (UPR) initiated by the transmembrane kinase/ribonuclease Ire1 has been implicated in a variety of diseases. Ire1, with its unique position in the UPR, is an ideal target for the development of therapies; however, the identification of specific kinase inhibitors is challenging. Recently, the development of covalent inhibitors has gained great momentum because of the irreversible deactivation of the target. We identified and determined the mechanism of action of the Ire1-inhibitory compound UPRM8. MS analysis revealed that UPRM8 inhibition occurs by covalent adduct formation at a conserved cysteine at the regulatory DFG+2 position in the Ire1 kinase activation loop. Mutational analysis of the target cysteine residue identified both UPRM8-resistant and catalytically inactive Ire1 mutants. We describe a novel covalent inhibition mechanism of UPRM8, which can serve as a lead for the rational design and optimization of inhibitors of human Ire1.

Introduction

The unfolded protein response (UPR) is a cellular protective mechanism that connects the presence of misfolded proteins in the endoplasmic reticulum (ER) to response mechanisms in the cytoplasm and nucleus.[1] Perturbation of this mechanism is involved in the pathogenesis of neurodegenerative, inflammatory, metabolic, and neoplastic diseases.[2] For example, the UPR is activated in some cancers, and Ire1 is directly implicated in multiple myeloma,[3] leukemia,[4] and pancreatic cancer.[5] These broad disease implications have generated considerable interest in UPR-targeting small molecules and their underlying mechanisms of action; this will be critical for proper preclinical validation of the UPR as a therapeutic target.

The UPR is initiated by Ire1, the transmembrane kinase/ribonuclease that is activated by the accumulation of unfolded proteins in the ER.[6] This leads to trans-phosphorylation of the cytosolic kinase domain of Ire1.[7] This has been proposed to increase access to its nucleotide-binding pocket, and binding of ATP or ADP to this open pocket results in the formation of back-to-back dimers.[8] This activates the Ire1 C-terminal ribonuclease domain, which catalyzes a nonconventional splicing event to remove an intron in the mRNA of a UPR transcriptional activator (Hac1 in yeast, XBP1 in metazoans).[9] The activator then translocates to the nucleus, where it binds to unfolded protein response elements (UPREs, by Hac1) or ER stress response elements (ERSEs, by XBP1) and induces the expression of genes involved in protein folding, glycosylation, secretion, membrane biogenesis, and ER-associated degradation (ERAD).[10]

Kinase-inactivating mutations of Ire1 severely compromise UPR signaling,[7] and structural studies have elucidated how nucleotide-competitive ligands can stimulate Ire1 ribonuclease: Mg^{2+}-dependent binding of nucleotides or Mg^{2+}-independent binding of synthetic kinase inhibitors allosterically stimulate Ire1 ribonuclease by inducing structural rearrangements in the kinase segment, thereby resulting in formation of back-to-back Ire1 dimers and subsequent higher-order oligomers.[8a, 11] This cofactor-assisted ribonuclease activation mechanism was further refined by the demonstration that different types of kinase inhibitors could have opposing effects on Ire1α: type I inhibitors stimulate, whereas type II inhibitors impede, ribonuclease activation.[12] It has become evident that Ire1 kinase conformation can be controlled by manipulation of the DFG-containing activation loop by appropriate kinase ligands, thus controlling Ire1 ribonuclease activity.

Most known kinase inhibitors are ATP-competitive and often exhibit a degree of polypharmacology. One strategy to make them more specific is to develop covalent inhibitors that depend on specific residues adjacent to the active site.[13] The

[a] Dr. D. D. Waller, Prof. Dr. M. Sebag
Department of Medicine, McGill University
1001 Boulevard Décarie, Montréal, QC H4A 3J1 (Canada)
E-mail: daniel.waller@mail.mcgill.ca

[b] Dr. D. D. Waller, Dr. G. Jansen, C. Martel-Lorion, Dr. K. Dejgaard, Prof. Dr. D. Y. Thomas
Department of Biochemistry, McGill University
3655 Promenade Sir William Osler, Montréal, QC H3G 1Y6 (Canada)

[c] Dr. M. Golizeh, T. C. Shiao, Prof. Dr. R. Roy, Prof. Dr. L. Sleno
Pharmaqam, Département de Chimie, Université du Québec à Montréal
Montréal, QC H3C 3P8 (Canada)

[d] Dr. J. Mancuso, Prof. Dr. Y. S. Tsantrizos
Department of Chemistry, McGill University
801 Sherbrooke St. West, Montréal, QC H3G 1Y6 (Canada)

Supporting information and the ORCID identification number(s) for the author(s) of this article can be found under http://dx.doi.org/10.1002/cbic.201500485.

search for covalent inhibitors and exploitation of appropriate nucleophilic residues to make more-specific kinase inhibitors is a promising strategy.[14]

Here we show that UPRM8, a pyrimidinedione, inhibits kinase (and thereby ribonuclease) activities in vitro of yeast and human Ire1. UPRM8 inhibits yeast Ire1 by the formation of covalent adducts with a conserved cysteine (C832) in the kinase activation loop. Analysis of C832 mutants confirmed a covalent mechanism of action for UPRM8 and thus demonstrates that the catalytic activities of Ire1 can be controlled by manipulation of the DFG+2 cysteine residue.

Results and Discussion

DFG+2 residue: A regulatory site to control kinase activation

We approached our goal of identifying novel covalent mechanisms to inhibit Ire1 by exploring the conservation of kinase activation loop residues between the DFG and APE motifs, because type II kinase inhibitors that reinforce the "DFG-out" configuration have been shown to block Ire1 ribonuclease activation.[12] The DFG+2 position immediately stood out as a site of interest, because the vast majority of kinases contain small amino acids (alanine or serine) at this position, whereas several inactive pseudokinases contain bulkier residues like phenylalanine or lysine (Figure 1A). Ire1 was among a subset of kinases that contain nucleophilic cysteines at DFG+2; this cysteine is conserved among Ire1 orthologues (Figure 1B). Our strategy was to identify electrophilic "warheads" that covalently modify the DFG+2 cysteine, thereby disrupting normal activation-loop regulation of Ire1 (Figure 1B). In order to identify such electrophilic warheads, we screened a small-molecule combinatorial library rich in electrophilic compounds. We performed this high-throughput screen in *Saccharomyces cerevisiae* with a UPR transcriptional reporter (Figure 1C) and identified a number of potential electrophilic molecules (UPR Modulators, UPRMs) that could prevent *HAC1* mRNA splicing by Ire1 in cells that were stressed with tunicamycin, a selective inhibitor of N-linked glycosylation and a potent UPR activator (Figure 1D).

UPRM8 inhibits yeast Ire1 in vitro

We selected the pyrimidinedione UPRM8 (Figure 2A) to elucidate the mechanism of yeast Ire1 (yIre1) inhibition by electrophilic UPR modulators. In order to assess if UPRM8 prevents tunicamycin (TM)-induced *HAC1* mRNA splicing by interfering with the ribonuclease activity of yIre1, we measured the in vitro ribonuclease activity by fluorescence dequenching of a synthetic RNA substrate that contains the Ire1 splice site of *XBP1* mRNA.[8b] This synthetic RNA substrate contains the *XBP1* cleavage sequence in its loop region and a destabilized stem to permit liberation of a 5′-AlexaFluor-647 (AF647) fluorophore from a 3′-Black-Hole-Quencher-3 (BHQ3; Figure S1A in the Supporting Information). We ruled out any confounding effects of UPRM8 on the fluorescence readout of this dequenching assay: even at very high concentrations (25 and 100 μM),

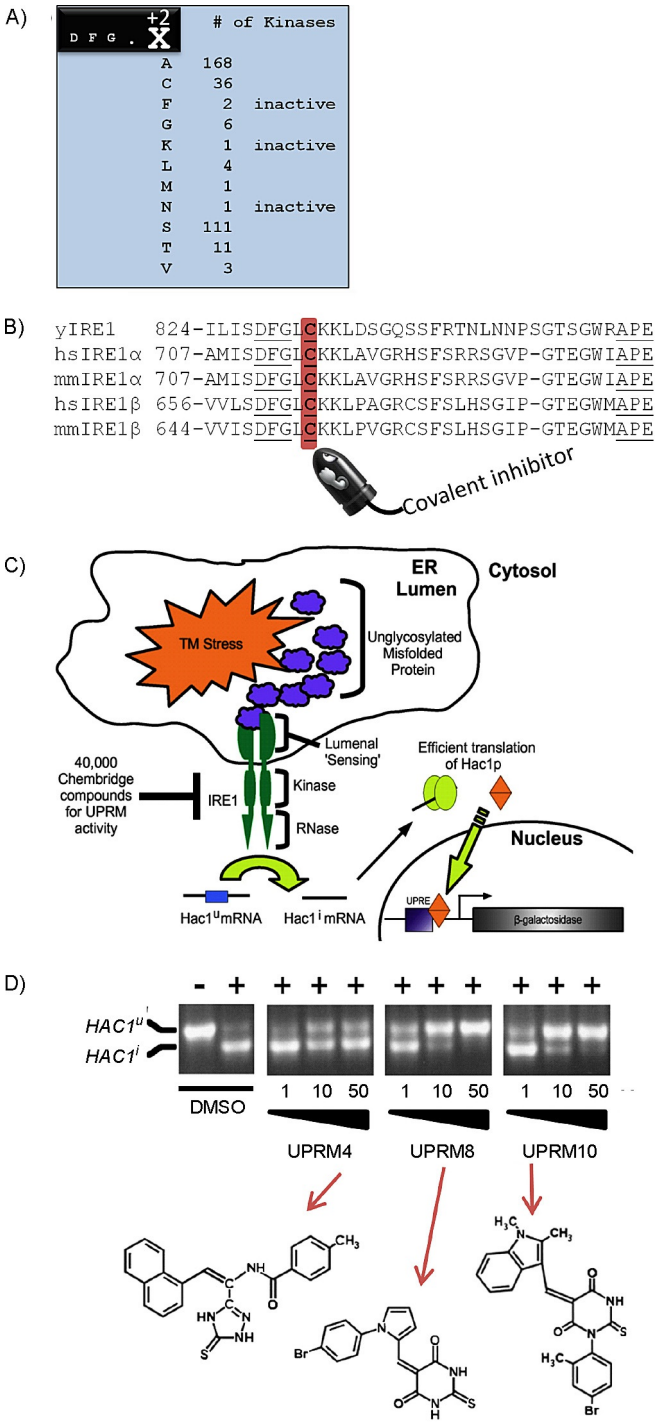

Figure 1. Rationale and strategy for screening for DFG+2 modifying compounds. A) Sequence alignment of human kinases with activation loops flanked by the conserved DFG and APE/SPE/PPE residues. Residues in the DFG position and the number of corresponding kinases are indicated. B) Sequence alignment of activation-loop residues of Ire1 orthologues showing conservation of the DFG+2 cysteine that will be targeted by covalent inhibition. C) Cartoon representation of the UPR transcriptional reporter screen to identify UPRMs. D) Three UPRMs and their effects on Ire1p-dependent HAC1 mRNA splicing. Left: negative (−, no TM) and positive (TM-only treatment) controls show the expected sizes of unspliced (HAC1u) and spliced (HAC1i) mRNA, respectively.

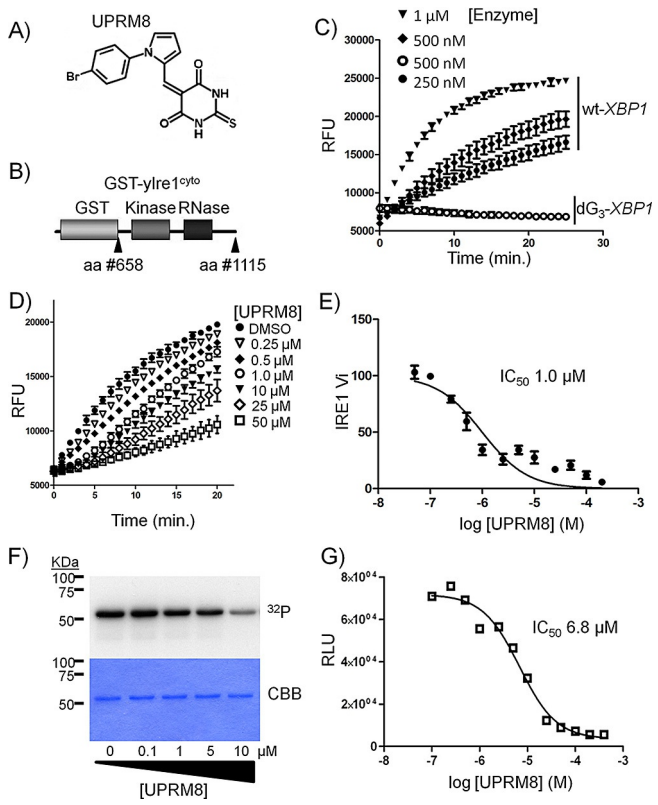

Figure 2. UPRM8 inhibits the dual enzymatic activities of ylre1^{cyto}. A) Chemical structure of UPRM8. B) Construct GST-ylre1^{cyto} was used to measure in vitro inhibition of yeast Ire1 ribonuclease activity by UPRM8. C) In vitro ribonuclease activity of purified GST-ylre1^{cyto} in *XBP1* fluorescence dequenching assays. dG$_3$-*XBP1*: mRNA probe that is not cleaved by Ire1 is shown to demonstrate specificity. D) The effect of increasing doses of UPRM8 on in vitro ribonuclease activity of GST-ylre1^{cyto} by fluorescence dequenching assays with substrate *XBP1* mRNA. E) Dose–response of UPRM8-mediated inhibition of GST-ylre1^{cyto} ribonuclease activity by plotting mean initial rate (RFU/second) of triplicate ribonuclease assays against log molar concentration of UPRM8. F) Standard [^{32}P]-ATP autophosphorylation assays with untagged ylre1^{cyto} demonstrate dose-dependent inhibition of ylre1^{cyto} autokinase activity by UPRM8. The Coomassie-stained image in the lower panel (CBB) confirms that equal amounts of enzyme were used. G) Dose–response and IC$_{50}$ of UPRM8 on in vitro autokinase activity of ylre1^{cyto} from ADP-Glo kinase assays. Data are mean ± SD (n = 3).

UPRM8 did not quench AF647 fluorescence (Figure S1 B). In order to measure Ire1 enzymatic activity we purified to homogeneity a recombinant protein comprising cytosolic residues of ylre1 with a GST fusion tag (GST-ylre1^{cyto}; Figure 2 B, Figure S1 C). Robust, concentration-dependent, ribonuclease activity was demonstrated for GST-ylre1^{cyto} in the dequenching assay (Figure 2 C). The absence of contaminating ribonuclease activities in our GST-ylre1^{cyto} preparation was demonstrated by the lack of fluorescence liberation when the *XBP1* mRNA stem-loop substrate was rendered incompatible for Ire1 cleavage by the presence of a 2′-deoxyribose-guanosine nucleotide 5′ of the Ire1 cleavage site[8b] (Figure 2 C). We clearly observed dose-dependent inhibition of the ribonuclease activity of GST-ylre1^{cyto} by UPRM8 (Figure 2 D). When the initial ribonuclease rates were plotted against the log of UPRM8 concentration, the resulting dose–response curve revealed an apparent IC$_{50}$ of 1.0 μM for UPRM8 (Figure 2 E). These results suggested that UPRM8 is a direct inhibitor of Ire1 ribonuclease activity.

Given that Ire1 ribonuclease activity can be controlled by nucleotide-competitive ligands that bind to the kinase active site,[11a,12,15] we wished to examine if a similar allosteric mechanism could underlie UPRM8 inhibition of Ire1 ribonuclease. To this end we tested the impact of UPRM8 on the autokinase activity of untagged ylre1^{cyto} in vitro, by using [γ-^{32}P]-ATP phosphotransfer (Figure 2 F) and ADP-Glo kinase assays (Figure 2 G). The results showed dose-dependent inhibition of ylre1 autophosphorylation by UPRM8 (IC$_{50}$ = 6.8 μM; Figure 2 G). Taken together, these results suggest that UPRM8 inhibits ylre1 ribonuclease activity by an allosteric mechanism that involves modulating the kinase segment in a way that inhibits its autophosphorylation.

UPRM8 inhibits the catalytic activities of human Ire1α

We next determined if UPRM8 also inhibits the catalytic activities of human Ire1α (hIre1) by using a cytosolic fragment purified from insect cells[16] (His$_6$-hIre1α^{cyto}; Figure 3 A and B). In the in vitro ribonuclease activity, evaluated in the fluorescence de-

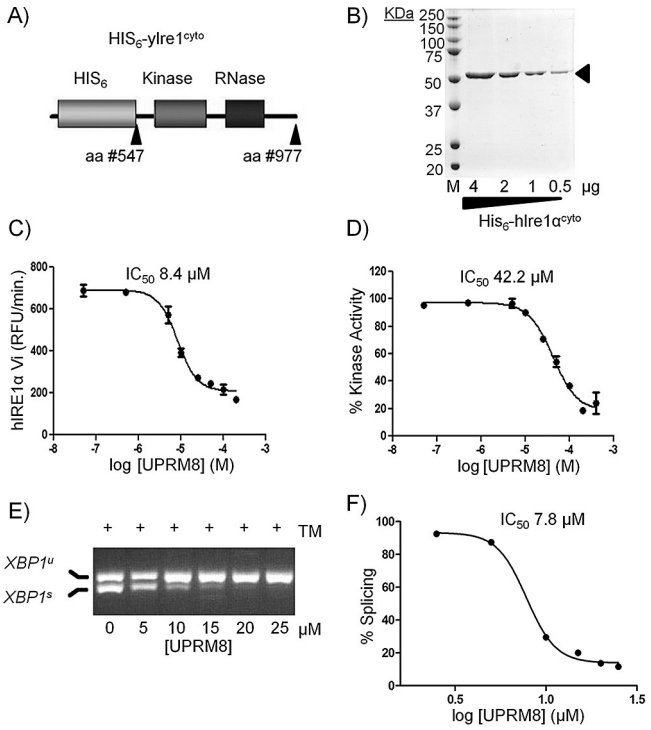

Figure 3. UPRM8 inhibits kinase and ribonuclease activities of human Ire1α. A) His$_6$-hIre1α^{cyto} construct used to measure in vitro inhibition of hIre1 ribonuclease activity by UPRM8. B) Coomassie-stained SDS-PAGE of His$_6$-hIre1α^{cyto} purified to homogeneity, as used for in vitro studies. C) Dose–response of UPRM8: mean initial velocities of His$_6$-hIre1α^{cyto} ribonuclease activity are plotted against log UPRM8 concentration (n = 3). D) Dose–response of UPRM8 on in vitro autophosphorylation of His$_6$-hIre1α^{cyto} from ADP-Glo kinase assays (mean ± SD, n = 3). E) RT-PCR assay demonstrates the effect of UPRM8 on *XBP1* mRNA splicing in 5 μg mL^{-1} TM-stressed HeLa cells. F) Densitometry analysis of *XBP1* RT-PCR products from panel E used for quantification and dose–response of UPRM8 on *XBP1* splicing in TM-stressed HeLa cells.

quenching assay, His_6-hIre1α^{cyto} exhibited concentration-dependent cleavage of the *XBP1* mRNA substrate (Figure 3C), but it had no effect on the mutant dG_3-*XBP1* mRNA control (Figure S2). Increasing concentrations of UPRM8 revealed dose-dependent inhibition (Figure 3D). The mean initial rates from triplicate experiments yielded $IC_{50} \approx 8.4\ \mu M$ (Figure 3C). When similar dose–response experiments with UPRM8 were tested on the in vitro autophosphorylation activity of His_6-hIre1α^{cyto}, we obtained $IC_{50} = 42.2\ \mu M$ (Figure 3D). We preincubated UPRM8 for 5 min with enzyme to allow covalent adduct formation prior to the addition of RNA substrate and reducing reagent. Together, these results show that UPRM8 can inhibit the kinase and ribonuclease activities of hIre1 in vitro, but the inhibition is less potent than with yIre1.

Finally, we evaluated the activity of UPRM8 on *XBP1* mRNA splicing in stressed HeLa cells. We performed a dose–response experiment by exposing HeLa cells to $5\ \mu g\,mL^{-1}$ TM (an ER stress inducer) and increasing concentrations of UPRM8. Following this co-treatment, we monitored *XBP1* mRNA splicing by RT-PCR (Figure 3E). The results showed reduced *XBP1* splicing with increasing doses of UPRM8. Next, we quantified the RT-PCR products by densitometry, in order to determine the percentage of *XBP1* splicing for each concentration of UPRM8 (data expressed relative to splicing for HeLa cells that received TM stressor but no inhibitor; Figure 3F). The IC_{50} of UPRM8 on *XBP1* mRNA in TM-stressed HeLa cells was 7.8 μM, remarkably similar to that obtained for UPRM8 in the in vitro ribonuclease activity of purified His_6-hIre1α^{cyto}. These results confirm that UPRM8 inhibits the dual enzymatic activities of both yeast and human Ire1.

Covalent addition of UPRM8 to C832 of yIre1^{cyto}

We noticed that a short preincubation (5 min) of yIre1^{cyto} with UPRM8 was necessary to obtain potent and reproducible inhibition curves. We also found that the potency of yIre1^{cyto} kinase inhibition by UPRM8 was unaffected by increasing concentrations of ATP in the autokinase reactions (Figure S1D) and that preincubation with the strong reducing reagent dithiothreitol abolished UPRM8 inhibition of yIre1^{cyto} (data not shown). These results suggested that UPRM8 is a covalent inhibitor, and we wondered if the electrophilic olefin connectivity between the pyrimidine and pyrrole heterocycles of UPRM8 acts as a Michael acceptor for a surface-exposed nucleophile in yIre1^{cyto}. To test this, we generated a reduced analogue of UPRM8 (UPRM8C; Figure 4A), in order to perform side-by-side comparison with UPRM8 for the ability to interfere with yIre1^{cyto} ribonuclease activity (Figure 4B). The results show no inhibition by UPRM8C at doses where UPRM8 impaired yIre1^{cyto} ribonuclease activity. The lack of inhibition by UPRM8C of yIre1^{cyto} ribonuclease activity strongly supports the hypothesis that UPRM8 acts as a Michael acceptor for yIre1^{cyto} nucleophiles.

In order to identify Ire1 nucleophilic residues that are modified by UPRM8, we performed peptide mass fingerprinting on yIre1^{cyto} that was exposed to UPRM8 prior to tryptic digestion and HPLC-MS/MS analysis. Untreated and UPRM8C-treated yIre1^{cyto} samples served as negative controls for adduct formation, so that we could restrict our analysis to UPRM8-specific adducts that underlie yIre1^{cyto} inhibition. Examination of the peak areas corresponding to the seven (unmodified) cysteine-containing tryptic fragments of untreated, UPRM8C-treated, and UPRM8-treated yIre1^{cyto} revealed reduction specifically in the abundance of the unmodified cysteine-832 peptide with UPRM8 treatment (Figure 4C). Manual analysis of MS/MS spectral data from the UPRM8-specific (bromine isotopic pattern positive) precursor ions at *m/z* 689.29 and 678.29 confirmed covalent addition of UPRM8 to this DFG+2 cysteine (Figure 4D and E). The identity of these two chemically distinct C832-UPRM8 adducts was further supported by comparison to spectra generated from a synthetic C832 tryptic peptide (Figure S3A and B). Synthetic versions of the acid and aldehyde metabolites of UPRM8 were generated, and their spectra corroborated the findings of our high resolution MS/MS data from the yIre1–UPRM8 incubation (Figure S3C and D). Thus UPRM8 behaves as a covalent (type IV)[17] kinase inhibitor of yIre1, by covalent modification of C832. In support of this result, we detected unmodified tryptic fragments for five of the six additional cysteine-containing peptides of yIre1^{cyto} (Table S1).

The detection of adducts on C832 but not at other cysteine residues in yIre1^{cyto} suggests that it is the predominant nucleophile stably modified by UPRM8; however, the reason for the selectivity for C832 is unclear. We hypothesize that the adjacent lysine residues allow formation of short-lived Schiff base species that could retain UPRM8 in close proximity to the C832 sulfhydryl side chain. It is possible that our fingerprinting experiments missed additional rare or transient UPRM8 adducts, so we decided to examine the activities of various C832 Ire1 mutants to establish the DFG+2 cysteine as the important UPRM8 modification site.

Mutagenesis reveals the importance of C832 for Ire1 catalytic function

The C832 residue is at the N-terminal end of the kinase activation loop, which contains canonical autophosphorylation sites that are known to be important for proper regulation of yIre1 kinase and ribonuclease activities. We inspected a crystal structure of yIre1^{cyto} (PDB ID: 2RIO)[8a] and found that C832 is distant from the ADP and Mg^{2+} ligands in this catalytically active structure (Figure 5A). This distance reinforces our hypothesis that UPRM8 does not behave as a prototypical nucleotide-competitive inhibitor of yIre1^{cyto} kinase. Rather, we suggest that UPRM8 adduct formation at C832 inhibits Ire1 by preventing its kinase activation segment from correctly adopting the "DFG-in" configuration that is characteristic of active (phosphorylated) kinases.[18]

In order to confirm the importance of the DFG+2 cysteine for the catalytic functions of yIre1, we performed site-directed mutagenesis on the *Escherichia coli* expression plasmid encoding GST-yIre1^{cyto} to obtain alanine, glutamic acid, serine, or lysine at position 832. We also generated a kinase-crippled yIre1-D828A mutant[15,19] to serve as a negative control for our in vitro assays. We purified wild-type and mutant yIre^{cyto} and

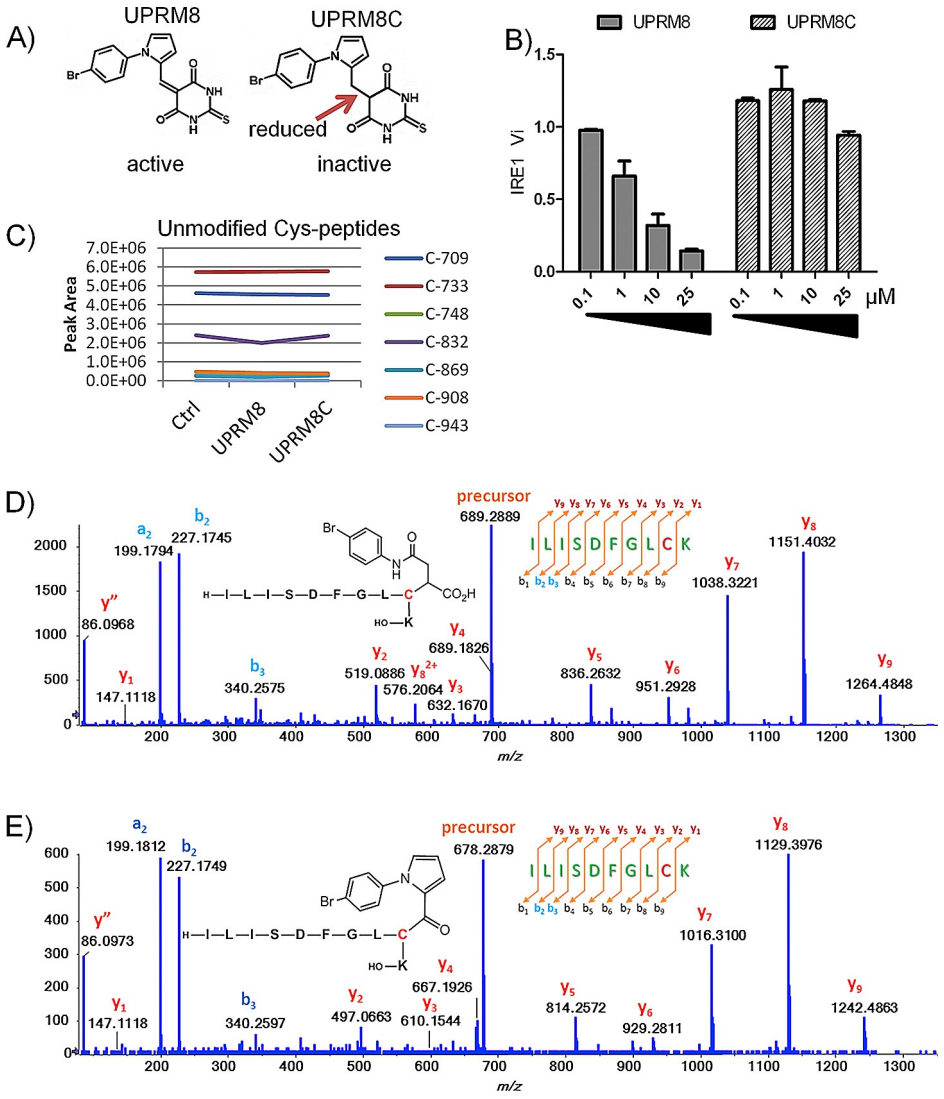

Figure 4. UPRM8 forms covalent adducts with C832 of ylre1^{cyto}. A) Chemical structure of UPRM8C, a reduced analogue of UPRM8. B) UPRM8 and UPRM8C affect mean initial velocity of GST-ylre1^{cyto} ribonuclease activity (IRE1 V_i) determined from fluorescence dequenching assays. Data are normalized to DMSO-treated controls (mean ± SD, $n = 3$). C) Integrated peak areas of cysteine-containing peptides from LC-MS/MS of trypsin-digested Ire1. A specific decrease in native C832 tryptic fragment of ylre1^{cyto} is evident only in the UPRM8-exposed sample. D) MS/MS of a bromine isotopic pattern-positive tryptic fragment of UPRM8-exposed ylre1^{cyto} (precursor 689.3 Da) allowed identification of a UPRM8 acid adduct at C832. E) Similarly, MS/MS of a second bromine fragment of UPRM8-exposed ylre1^{cyto} (precursor 678.3 Da) allowed identification of a UPRM8 aldehyde adduct at C832.

examined them by SDS-PAGE (Figure 5 B). The reduced electrophoretic mobility of wild-type and C832A and C832S mutants suggests that these are autophosphorylation-competent; the D828A, C832D, and C832K mutants appeared to have increased electrophoretic mobility, thus suggesting reduced autophosphorylation. To confirm these findings we performed standard [γ^{32}P]-ATP in vitro kinase assays on wild-type and mutant GST-ylRE1^{cyto} (Figure 5 C). The autophosphorylation activities of these mutants are largely consistent with their observed electrophoretic mobilities: wild-type, C832A, and C832S GST-ylre1^{cyto} were functional kinases, whereas C832K and D828A were inactive. Mutant C832D showed divergent results for the electrophoretic mobility and [γ^{32}P]-ATP kinase assays. This might have arisen from the increased sensitivity and specificity of the in vitro kinase assay, where C832D clearly showed almost wild-type autophosphorylation. Thus we conclude that C832D is indeed an active kinase. Overall, these results suggest that C832 might be a "sweet spot" for covalent inhibition.

Consequently, we assessed the in vitro ribonuclease activity of wild-type and mutant GST-ylre1^{cyto} with the fluorescence dequenching assay (Figure 5 D). This resulted in the following ylre1 ribonuclease activities: wild-type, C832A, and C832S mutants displayed robust ribonuclease activity, whereas C832D, C832K, and D828A showed severely crippled ribonuclease function. This difference in ribonuclease activity was further demonstrated by comparing mean initial rates in duplicate fluorescence dequenching experiments (Figure 5 E). The cause for divergent in vitro kinase and ribonuclease activities for the C832D mutant remains unresolved; however, this mutant

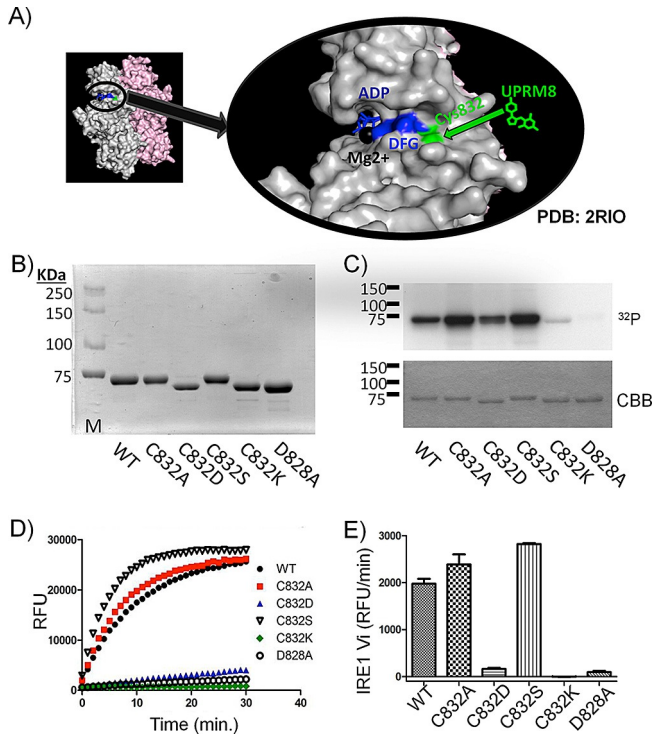

Figure 5. Mutation of C832 affects the enzymatic activity of yIre1^{cyto}. A) Arrow indicates UPRM8 covalent action at Cys832 (surface in green). Note the proximity of Cys832 to the conserved kinase DFG motif (blue), which is known to coordinate Mg2+ (black sphere), which allows binding of nucleotide ligand (ADP, blue). This structural depiction was rendered based on the crystal structure of yeast IRE1^{cyto} (PDB ID: 2RIO). B) Electrophoretic mobility of purified C832 yIre1^{cyto} mutants by SDS-PAGE (6%). C) [γ-^{32}P]-ATP autophosphorylation assays confirm impaired in vitro autokinase activity of C832D and C832K GST-yIre1^{cyto} mutants. Wild-type and kinase-deficient (D828A) GST-yIre1^{cyto} served as positive and negative controls, respectively. D) In vitro ribonuclease activity of GST-yIre1^{cyto} mutants examined by fluorescence dequenching assays with the *XBP1* probe. E) Initial ribonuclease velocities of C832 mutants, as determined by dequenching assays (mean ± SD, $n = 3$).

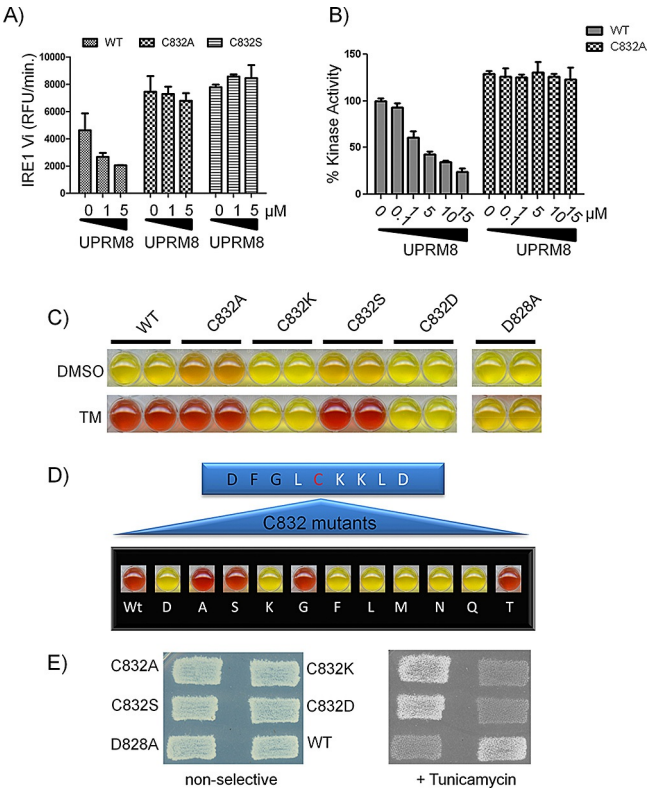

Figure 6. Ire1-C832A and -C832S mutants are resistant to UPRM8 and complement ire1Δ yeast. A) In vitro ribonuclease assays demonstrate that the enzymatically sufficient C832A and C832S GST-Ire1^{cyto} mutants are resistant to UPRM8 inhibition (mean ± SD, $n = 3$). B) Increasing doses of UPRM8 do not impair autophosphorylation by mutant C832 GST-Ire1^{cyto}. Wild-type GST-Ire1^{cyto} served as a positive control. C) The integrity of UPR signaling is assessed by transforming the ire1Δ UPR reporter yeast strain with the indicated Ire1 plasmids. TM was used to induce ER stress (negative control, DMSO). Wild-type and D828 IRE1 plasmids served as positive and negative controls, respectively. D) UPR complementation by a broader panel of IRE1-C832 missense mutants by using the same ire1Δ *UPRE::lacZ* transcriptional reporter assay. All strains were exposed to TM to induce ER stress. E) UPR complementation by IRE1-C832 plasmids is confirmed by growth on TM-containing medium.

showed increased electrophoretic mobility, similarly to the kinase-crippled C832K and D828A mutants, and it also shares their severely defective ribonuclease ability. Therefore, it is clear that the kinase segment of C832D does not fulfill its role to properly regulate the Ire1 conformational state that normally controls dimer/oligomer formation during ribonuclease activation. It should also be noted that the C832A and C832S mutants demonstrate slightly elevated kinase and ribonuclease activity when compared to wild-type, thus suggesting that these are Ire1-activating mutations. Taken together, these results show that genetic manipulation of C832 provides a mechanism to allosterically regulate the kinase and ribonuclease functions of yIre1.

C832A and C832S mutants of yIre1 are resistant to UPRM8

The intact enzymatic activities of mutants yIre1-C832A and -C832S afforded the opportunity to test whether the DFG+2 sulfhydryl nucleophile of yIre1 is required for UPRM8 inhibition. We first evaluated the impact of 0, 1, and 5 μM UPRM8 on the initial rates of wild-type, C832A, and C832S GST-yIre1^{cyto} in the fluorescence dequenching assay (Figure 6A). The results again demonstrate that the C832A and C832S mutants have elevated ribonuclease activity and are more resistant to UPRM8 inhibition when compared to wild-type yIre1. We tested if the absence of a cysteine nucleophile at position 832 could also circumvent UPRM8 inhibition of yIre1 kinase. To do this we compared wild-type and C832A yIre1^{cyto} in the dose–response of UPRM8 for in vitro autokinase activity (Figure 6B). C832A kinase activity was again elevated compared to wild-type, and furthermore was unaffected by UPRM8 at doses where robust inhibition of wild-type yIre1^{cyto} were observed. These results strongly support the covalent mechanism of action of UPRM8 at C832. A contribution by other UPRM8 adducts to yIre1 inhibition cannot be entirely excluded, but the consistently increased enzymatic activity and decreased sensitivity of yIre1^{cyto}-C832A and -C832S to UPRM8 inhibition shows that we have identified the important covalent modification site.

To confirm C832 as a valid access point for manipulating UPRs in stressed cells, we generated alanine, lysine, serine, and aspartate replacement mutants in full-length yIre1. These mutants allowed us to assess UPR induction in *S. cerevisiae* by colorimetric monitoring (yellow to red) of the conversion of β-galactosidase substrate chlorophenol red-β-D-galactopyranoside. The resulting transcriptional reporter activity was measured in the presence (TM in Figure 6C) and absence (DMSO) of an exogenous ER stress insult. As expected, TM-induced UPR reporter activation was rescued in *S. cerevisiae* ire1Δ cells that were transformed with the wild-type *yIRE1* plasmid; it was not rescued by the kinase-inactivated yIre1-D828A plasmid. The UPRM8-resistant mutants yIre1-C832A and yIre1-C832S restored UPR reporter activity in response to TM and also showed above-wild-type background UPR activation, even in the absence of stressor, thus confirming our in vitro findings that indicated that mutations C832A and C832S are Ire1-activating. As expected from the in vitro ribonuclease activities, yIre1 mutants C832K and C832D failed to rescue UPR transcriptional activation. Evaluation of a wider panel of C832 mutants by this UPR transcriptional reporter assay suggested that size (rather than charge) of the amino acid side chain at position 832 is critical for yIre1 function (Figure 6D). As predicted from our in vitro results, mutants C832A and C832S produced basal and stress-induced UPR reporter activation that was largely insensitive to UPRM8 (Figure S4). Together, these results show that the DFG+2 residue of yIre1 is important for UPR signal transmission and that mis-sense mutants with bulky side chains at residue 832 fail to complement the UPR in ire1Δ yeast.

Functional characterization of C832 mutants in vivo

In order to confirm the inability of mutants yIre1-C832K and yIre1-C832D to complement the UPR in ire1Δ cells, we determined their ability to restore growth on TM-containing solid-medium plates (Figure 6E). The results were in agreement with those for the UPR transcriptional reporter assay and the phenotypic assessment of the UPR: yIre1-C832A and yIre1-C832S are enzymatically competent and can complement the UPR in ire1Δ cells, whereas yIre1-C832K and yIre1-C832D have deficient ribonuclease activity and cannot initiate a robust UPR. Of note, the stress-independent activation seen for C832A and C832S mutants in the transcriptional reporter assay did not result in an obvious growth advantage in this assay; however, patch-growth assays on solid agar plates are not well suited for quantification of subtle fitness phenotypes. Further studies are needed to evaluate if the mild stress-independent UPR activation afforded by the C832A and C832S mutants can precondition cells to better tolerate an acute ER stress insult.

Importantly, the in vitro ribonuclease activities of the various Ire1 mutants tested here universally correlated with their ability to functionally complement the UPR in ire1Δ yeast. These results show that UPRM8 adducts at C832 (or bulky side chains of the ribonuclease-inactive C832K and C832D mutants) cause steric hindrances that prevent normal activation-loop regulation of yIre1. We believe this failure to regulate the kinase segment of yIre1 prevents it from fulfilling its key role as a nucleotide-responsive scaffold to promote dimerization and subsequent oligomerization, steps that are important for Ire1 ribonuclease activity.[8a,11,19b] Our results suggest that UPRM8 acts as a type IV kinase inhibitor by covalent modification of the DFG+2 cysteine, and that this impairs yIre1 ribonuclease by reinforcing an inactive "DFG-out" kinase configuration. This allosteric mechanism of ribonuclease inhibition by UPRM8 is similar to, but distinct from, the allosteric mechanism that was demonstrated for type II inhibitors of human Ire1α.[12]

Conclusions

Our mechanistic studies on UPRM8 inhibition of yIre1 support the development of kinase-directed inhibitors for hIre1 by exploiting the analogous DFG+2 nucleophile (C715) that lies well outside the conserved ATP pocket. We feel that this strategy will allow the identification of more-selective inhibitors of hIre1 than would be found among traditional ATP-competitive ligands, which are plagued by specificity concerns. FDA approval of ibrutinib and afatinib in chronic lymphocytic leukemia and non-small-cell lung cancer, respectively, substantiates the use of cysteine-directed covalent inhibitors in the clinic, and our results imply that bulky C715-directed covalent ligands should be capable of allosterically inactivating the dual enzymatic activities of hIre1.

In summary, we have described the identification and characterization of UPRM8, a covalent inhibitor of yeast and human Ire1. Our mechanistic studies on UPRM8 revealed the importance of the DFG+2 cysteine residue for yIre1 catalytic function and UPR signaling. We have clearly demonstrated that the DFG+2 nucleophile can be manipulated, either chemically or genetically, in order to allosterically control yIre1 ribonuclease. This work provides a novel covalent inhibition strategy that can be exploited in future work to develop potent and selective inhibitors of human Ire1α.

Experimental Section

Chemicals: UPRM8 (5-([1-(4-bromophenyl)-1*H*-pyrrol-2-yl]methylene)-2-thioxodihydro-4,6(1*H*,5*H*)-pyrimidinedione), identified in a high-throughput screen, was purchased from Chembridge (#6314300; San Diego, CA). The reduced analogue, UPRM8C, was synthesized from UPRM8 as follows. UPRM8 (50 mg, 0.133 mmol) was dissolved in methanol (5 mL), then sodium borohydride (5.0 mg, 1 equiv, 0.133 mmol) was added in a single portion. The reaction stirred at room temperature for 2 h. Solvent was removed in vacuo, and the residue was diluted with water. The pH was neutralized with HCl (1 M), and the solid that formed was filtered and dried in vacuo to yield 39 mg (78%) of 5-((1-(4-bromophenyl)-1*H*-pyrrol-2-yl)methyl)-2-thioxodihydropyrimidine-4,6(1*H*,5*H*)-dione (UPRM8C) as a white powder.

In vitro kinase and ribonuclease assays: Autophosphorylation of yIre1^{cyto} and C832 mutants was monitored by standard [γ-^{32}P]-ATP kinase assays (described previously)[20] or ADP-Glo kinase assays according to the manufacturer's (Promega) instructions. Purified yeast GST-yIre1^{cyto} or His$_6$-hIre1α^{cyto} was used in a fluorescence-based ribonuclease assay to monitor Ire1-dependent cleavage of

a synthetic dual-labeled AlexaFluor647 (AF647) and Black Hole Quencher 3 (BHQ3) RNA substrate (synthesized by either Invitrogen or Biosearch Technologies).[8b] Assays were carried out as described previously,[8b] with a minor modification: GST-yIre1^{cyto} (500 nM) or His$_6$-hIre1α^{cyto} (50 nM) was preincubated for 5 min in RNase buffer (HEPES (20 mM, pH 7.4), MgOAc (1 mM), KOAc (50 mM)) with twice the indicated concentrations of UPRM8, prior to addition of an equal volume of RNase buffer supplemented with DTT (2 mM), ADP (4 mM), and *XBP1* AF647/BHQ3 probe (2 μM). Final reaction volumes were 50 μL, and the fluorescence produced by Ire1^{cyto}-liberated AF647 fluorophore was monitored in a SynergyMx plate reader (BioTek, Winooski, VT).

Yeast plasmids, strains, and media: *S. cerevisiae* was cultured in rich medium (YPD), or synthetic drop-out medium (SD); agar (2%) was added for solid media. The reporter strain CML8-1-ire1Δ was generated by first integrating the upre-*lacZ-URA3* cassette into the drug-sensitive strain AD1–8.[21] In order to facilitate chromosomal integration of the cassette into the *ura3* locus of AD1-8, plasmid pLG-178-UPRE-Y-355[22] was first linearized with StuI and then transformed into AD1-8 by standard techniques.[23] The resulting strain (CML8-1) was subjected to gene replacement at the *IRE1* locus by integration of a nourseothricin-resistance marker (natMX), to create CML8-1-ire1Δ::natMX his1 UPRE-Y-CYC1-LacZ::ura3-52. CML8–1 ire1Δ was then transformed with centromeric vectors containing *IRE1*-promoter-controlled *IRE1* wild-type, or *IRE1* mutants (C832A/D/F/G/K/L/M/N/Q/S/T, D828A), which were generated by PCR mutagenesis, and subsequently in vivo recombined into pGREG-HIS1. The same mutant set was generated in a *LEU2*-marker-based plasmid pGREG505 and used in the ire1Δ yeast two-hybrid strain YG574 for the TM-sensitivity assays,[24] in order to simultaneously assess growth on non-selective (SD-Leu) and selective (SD-Leu supplemented with TM (2 μg mL^{-1})) solid-media plates.

Yeast β-galactosidase screen assay: An overnight culture of UPR reporter yeast was diluted to $OD_{600} = 0.5$ and incubated at 30 °C for 2 h. This culture was then diluted to $OD_{600} = 0.15$ and then transferred to 96-well plates that were preloaded with 50 μL of the following 4× solution: sodium phosphate buffer (400 mM, pH 7.0) in SD-Ura medium that contained either DMSO (2%) or TM (8 μg mL^{-1}). The plates were sealed, stacked, and incubated at 30 °C with gentle shaking for 3 h. Next, 20 μL of 10× CPRG-SDS solution (chlorophenol-red-β-D-galactopyranoside (1 mg mL^{-1}), SDS (0.0625%)) was added to each well by a Microfill automatic dispenser (Biotek) and incubated for 3 h at 30 °C. Plates were centrifuged, and the supernatants were transferred to fresh 96-well plates prior to scanning. The final assay volumes were 200 μL; final concentrations of each reagent in SD-Ura medium were: sodium phosphate (100 mM, pH 7.0), TM (2 μg mL^{-1}) or DMSO (0.5%), CPRG (100 μg mL^{-1}), and SDS (0.00625%). Details on the high throughput chemical screen and hit-selection criteria are in the Supporting Information.

Cell culture and Semi-quantitative RT-PCR of XBP1 mRNA: HeLa cells were maintained at 37 °C, under CO_2 (5%) in DMEM supplemented with FBS (10%). Cultured cells were stressed by addition of TM (5 μg mL^{-1}) in the presence of the indicated concentration of UPRM8, and incubated for 2 h. Examination of *XBP1* mRNA splicing by RT-PCR was described previously.[25] RT-PCR products were separated by electrophoresis in 2% agarose gels followed by ethidium bromide staining. Densitometry of the spliced and unspliced *XBP1* PCR products was performed by Quantity One image analysis software (Bio-Rad).

Acknowledgements

We would like to thank Maruf Ali (Imperial College London) for graciously sharing his baculovirus construct for expression of human Ire1α. This work was funded by grants from the Canadian Institutes for Health Research (CIHR; grant no. 234170 and 218654) and Le Réseau québécois de Recherche sur les Medicaments. D.D.W. was supported by a CIHR STIHR Chemical Biology training scholarship.

Keywords: endoplasmic reticulum stress · enzyme catalysis · inhibitors · Ire1 · type IV kinase inhibitor · Xbp1

[1] D. Ron, P. Walter, *Nat. Rev. Mol. Cell Biol.* **2007**, *8*, 519–529.
[2] S. Wang, R. J. Kaufman, *J. Cell Biol.* **2012**, *197*, 857–867.
[3] a) N. Mimura, M. Fulciniti, G. Gorgun, Y.-T. Tai, D. Cirstea, L. Santo, Y. Hu, C. Fabre, J. Minami, H. Ohguchi, T. Kiziltepe, H. Ikeda, Y. Kawano, M. French, M. Blumenthal, V. Tam, N. L. Kertesz, U. M. Malyankar, M. Hokenson, T. Pham, et al., *Blood* **2012**, *119*, 5772–5781; b) I. Papandreou, N. C. Denko, M. Olson, H. Van Melckebeke, S. Lust, A. Tam, D. E. Solow-Cordero, D. M. Bouley, F. Offner, M. Niwa, A. C. Koong, *Blood* **2011**, *117*, 1311–1314; c) M. Ri, E. Tashiro, D. Oikawa, S. Shinjo, M. Tokuda, Y. Yokouchi, T. Narita, A. Masaki, A. Ito, J. Ding, S. Kusumoto, T. Ishida, H. Komatsu, Y. Shiotsu, R. Ueda, T. Iwawaki, M. Imoto, S. Iida, *Blood Cancer J.* **2012**, *2*, e79.
[4] a) B. K. Masouleh, H. Geng, C. Hurtz, L. N. Chan, A. C. Logan, M. S. Chang, C. Huang, S. Swaminathan, H. Sun, E. Paietta, A. M. Melnick, P. Koeffler, M. Müschen, *Proc. Natl. Acad. Sci. USA* **2014**, *111*, E2219–2228; b) C.-H. Tang, S. Ranatunga, C. L. Kriss, C. L. Cubitt, J. Tao, J. A. Pinilla-Ibarz, J. R. Del Valle, C.-C. A. Hu, *J. Clin. Invest.* **2014**, *124*, 2585–2598.
[5] W. Chien, L.-W. Ding, Q.-Y. Sun, L. A. Torres-Fernandez, S. Z. Tan, J. Xiao, S. L. Lim, M. Garg, K. L. Lee, S. Kitajima, S. Takao, W. Z. Leong, H. Sun, I. Tokatly, L. Poellinger, S. Gery, P. H. Koeffler, *Oncotarget* **2014**, *5*, 4881–4894.
[6] B. M. Gardner, P. Walter, *Science* **2011**, *333*, 1891–1894.
[7] C. E. Shamu, P. Walter, *EMBO J.* **1996**, *15*, 3028–3039.
[8] a) K. P. K. Lee, M. Dey, D. Neculai, C. Cao, T. E. Dever, F. Sicheri, *Cell* **2008**, *132*, 89–100; b) R. L. Wiseman, Y. Zhang, K. P. K. Lee, H. P. Harding, C. M. Haynes, J. Price, F. Sicheri, D. Ron, *Mol. Cell* **2010**, *38*, 291–304.
[9] a) C. Sidrauski, P. Walter, *Cell* **1997**, *90*, 1031–1039; b) H. Yoshida, T. Matsui, A. Yamamoto, T. Okada, K. Mori, *Cell* **2001**, *107*, 881–891.
[10] K. J. Travers, C. K. Patil, L. Wodicka, D. J. Lockhart, J. S. Weissman, P. Walter, *Cell* **2000**, *101*, 249–258.
[11] a) A. V. Korennykh, P. F. Egea, A. A. Korostelev, J. Finer-Moore, R. M. Stroud, C. Zhang, K. M. Shokat, P. Walter, *BMC Biol.* **2011**, *9*, 48; b) A. V. Korennykh, P. F. Egea, A. A. Korostelev, J. Finer-Moore, C. Zhang, K. M. Shokat, R. M. Stroud, P. Walter, *Nature* **2009**, *457*, 687–693.
[12] L. Wang, B. G. K. Perera, S. B. Hari, B. Bhhatarai, B. J. Backes, M. A. Seeliger, S. C. Schürer, S. A. Oakes, F. R. Papa, D. J. Maly, *Nat. Chem. Biol.* **2012**, *8*, 982–989.
[13] J. Singh, R. C. Petter, T. A. Baillie, A. Whitty, *Nat. Rev. Drug Discovery* **2011**, *10*, 307–317.
[14] a) Q. Liu, Y. Sabnis, Z. Zhao, T. Zhang, S. J. Buhrlage, L. H. Jones, N. S. Gray, *Chem. Biol.* **2013**, *20*, 146–159; b) N. London, R. M. Miller, S. Krishnan, K. Uchida, J. J. Irwin, O. Eidam, L. Gibold, P. Cimermančič, R. Bonnet, B. K. Shoichet, J. Taunton, *Nat. Chem. Biol.* **2014**, *10*, 1066–1072; c) I. M. Serafimova, M. A. Pufall, S. Krishnan, K. Duda, M. S. Cohen, R. L. Maglathlin, J. M. McFarland, R. M. Miller, M. Frödin, J. Taunton, *Nat. Chem. Biol.* **2012**, *8*, 471–476.
[15] F. R. Papa, C. Zhang, K. Shokat, P. Walter, *Science* **2003**, *302*, 1533–1537.
[16] M. M. U. Ali, T. Bagratuni, E. L. Davenport, P. R. Nowak, M. C. Silva-Santisteban, A. Hardcastle, C. McAndrews, M. G. Rowlands, G. J. Morgan, W. Aherne, I. Collins, F. E. Davies, L. H. Pearl, *EMBO J.* **2011**, *30*, 894–905.
[17] J. R. Simard, S. Klüter, C. Grütter, M. Getlik, M. Rabiller, H. B. Rode, D. Rauh, *Nat. Chem. Biol.* **2009**, *5*, 394–396.

[18] a) L. N. Johnson, M. E. Noble, D. J. Owen, *Cell* **1996**, *85*, 149 – 158; b) A. P. Kornev, N. M. Haste, S. S. Taylor, L. F. ten Eyck, *Proc. Natl. Acad. Sci. USA* **2006**, *103*, 17783 – 17788.

[19] a) A. Chawla, S. Chakrabarti, G. Ghosh, M. Niwa, *J. Cell Biol.* **2011**, *193*, 41 – 50; b) A. V. Korennykh, A. A. Korostelev, P. F. Egea, J. Finer-Moore, R. M. Stroud, C. Zhang, K. M. Shokat, P. Walter, *BMC Biol.* **2011**, *9*, 47; c) K. Mori, W. Ma, M.-J. Gething, J. Sambrook, *Cell* **1993**, *74*, 743 – 756.

[20] C. Wu, M. Whiteway, D. Y. Thomas, E. Leberer, *J. Biol. Chem.* **1995**, *270*, 15984 – 15992.

[21] A. Decottignies, A. M. Grant, J. W. Nichols, H. de Wet, D. B. McIntosh, A. Goffeau, *J. Biol. Chem.* **1998**, *273*, 12612 – 12622.

[22] K. Mori, A. Sant, K. Kohno, K. Normington, M. J. Gething, J. F. Sambrook, *EMBO J.* **1992**, *11*, 2583 – 2593.

[23] G. Jansen, C. Wu, B. Schade, D. Y. Thomas, M. Whiteway, *Gene* **2005**, *344*, 43 – 51.

[24] a) G. Jansen, P. Määttänen, A. Y. Denisov, L. Scarffe, B. Schade, H. Balghi, K. Dejgaard, L. Y. Chen, W. J. Muller, K. Gehring, D. Y. Thomas, *Mol. Cell. Proteomics* **2012**, *11*, 710 – 723; b) S. Pollock, G. Kozlov, M.-F. Pelletier, J.-F. Trempe, G. Jansen, D. Sitnikov, J. J. M. Bergeron, K. Gehring, I. Ekiel, D. Y. Thomas, *EMBO J.* **2004**, *23*, 1020 – 1029.

[25] S. H. Back, M. Schröder, K. Lee, K. Zhang, R. J. Kaufman, *Methods* **2005**, *35*, 395 – 416.

Manuscript received: September 21, 2015

Accepted article published: January 21, 2016

Final article published: March 7, 2016